AIAA JOURNAL
Vol. 50, No. 9, September 2012

Robust Airfoil Optimization Using Maximum Expected Value and Expected Maximum Value Approaches

Ana-Maria Croicu*
Kennesaw State University, Kennesaw, Georgia 30144
M. Yousuff Hussaini†
Florida State University, Tallahassee, Florida 32306
Antony Jameson‡
Stanford University, Stanford, California 94305
and
Goetz Klopfer§
NASA Ames Research Center, Moffett Field, California 94035

DOI: 10.2514/1.J051467

Deterministic engineering design often leads to unexpected or physically unrealizable results. This is due to the fact that deterministic design is not able to capture the effects of even slight natural fluctuations of parameters. Deterministic transonic shape optimization is no exception: deterministic designs can result in dramatically inferior performance when the actual operating conditions are different from the design conditions used during a deterministic optimization procedure. The goal of this paper is to overcome the off-design performance degradation of deterministic transonic shape optimization by using two different optimization approaches to produce robust designs. Two criteria, the well-known maximum/minimum expected value criterion (MEV) and the alternative expected maximum/minimum value criterion (EMV), are studied and applied to improve an initial RAE 2822 design. It turns out that EMV is much easier to implement than MEV, given a deterministic optimization code, and may provide a promising method for optimizing design shapes under uncertainty.

I. Introduction

Optimization theory, one of the oldest and most mature branches of mathematics, has ubiquitous applications in scientific and engineering disciplines. The main goal of these real-world applications is finding the best choice (the optimum point) that yields the most desirable or satisfactory solution for certain criteria. For example, the optimum point could maximize performance or profitability, or it could minimize risk. The specific example studied in this paper is airfoil shape design, where the objective is to select an airfoil geometry that minimizes the drag coefficient for a given lift.

Traditional gradient-based optimization methods based on finite difference derived gradients [1,2] are not very computationally efficient. With current advances in computational fluid dynamics and modern computers, however, aerodynamic design optimization becomes more feasible than ever, and has been extensively investigated in recent years. Optimization techniques based on adjoint methods [3–6], evolutionary algorithms, or stochastic algorithms [7–10] have been developed and implemented.

The adjoint method is extremely efficient when used with a gradient-based optimization technique, since the necessary gradients are obtained via the solution of the adjoint equations of the governing equations of interest. The computational cost incurred in the calculation of the complete gradient is independent of the number of design variables, and is similar to that of the flow solution. There are a number of partial derivatives that must be evaluated in the adjoint method that do depend on the number of variables, but they are not computationally expensive. The adjoint method was applied in this way to elliptical equations for shape design by Pironneau [11], and was first used in transonic flow by Jameson [12]. Since then, this method has become a popular tool for aerodynamic optimization [3–6]. Unfortunately, there is a drawback associated with the gradient-based methods, and implicitly with the adjoint method: they may get trapped in local minima.

To overcome this, stochastic methods such as genetic algorithms, simulated annealing algorithms, and so on have been applied to aerodynamic shape design. Although these algorithms were inspired by different natural processes, their application to optimization problems shares a common feature: the search for the global optimum through a stochastic process. Genetic algorithms belong to a class of methods called evolutionary algorithms, and they are inspired by the process of natural selection. These evolutionary algorithms have been applied to airfoil shape design by Quagliarella and Cioppa [13], Yamamoto and Inoue [14], and recently by de Sousa and Ramos [8], and Liu [10]. Simulated annealing algorithms, on the other hand, are inspired by the behavior of a collection of atoms immersed in a heat bath subject to a cooling schedule. Aly et al. [15] and Wang et al. [7] have applied annealing algorithms to the design of an optimal aerodynamic shape. The main disadvantage of all these stochastic algorithms is that they usually require a great number of evaluations of the objective function.

Unfortunately, despite the "stochastic" name, all of the aforementioned methods are deterministic in that the conditions or parameters of the problem are all known or predetermined. In reality, the conditions or parameters of the problem under investigation might not be all known beforehand or might be variable due to naturally occurring and irreducible fluctuations. The uncertainty is said to be epistemic in the former case and aleatory in the latter case [16]. In such a situation, optimization is said to be under "uncertainty," and the notion of "optimum" is not well understood.

To the authors' knowledge, optimization under uncertainty is quite new in airfoil optimization. Several different approaches can be

Received 30 June 2011; revision received 1 February 2012; accepted for publication 1 February 2012.

*Associate Professor of Mathematics, Department of Mathematics and Statistics.
†Sir James Lighthill Professor of Mathematics and Computational Science and Engineering, Department of Mathematics. Fellow AIAA.
‡Thomas V. Jones Professor of Engineering, Department of Aeronautics and Astronautics. Fellow AIAA.
§Research Scientist.

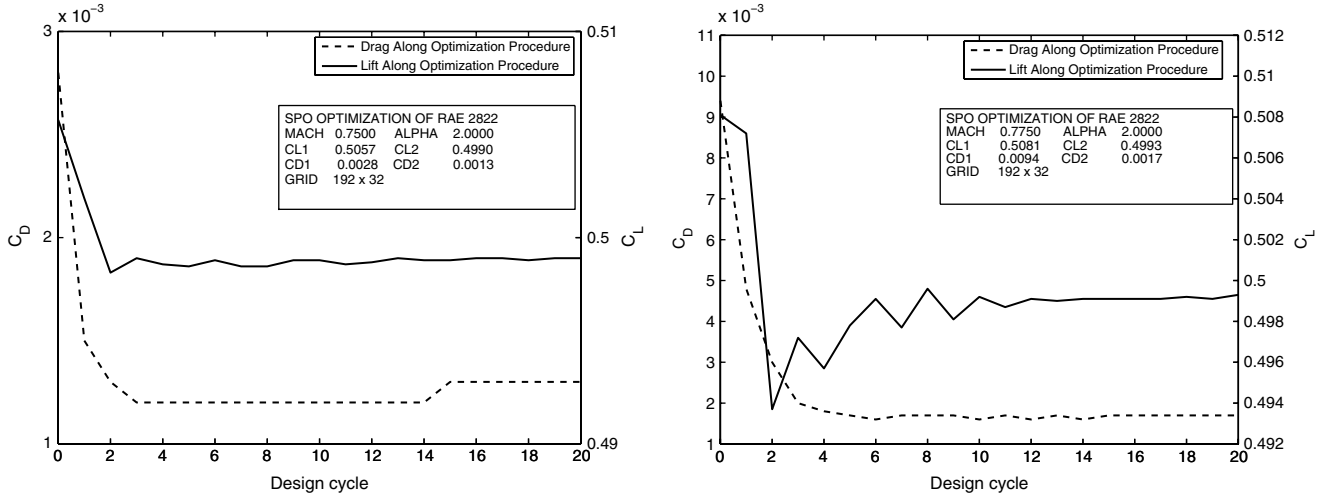

a) M=0.75 **b) M=0.775**

Fig. 1 Drag and lift convergence along 20 design cycles for the SPO.

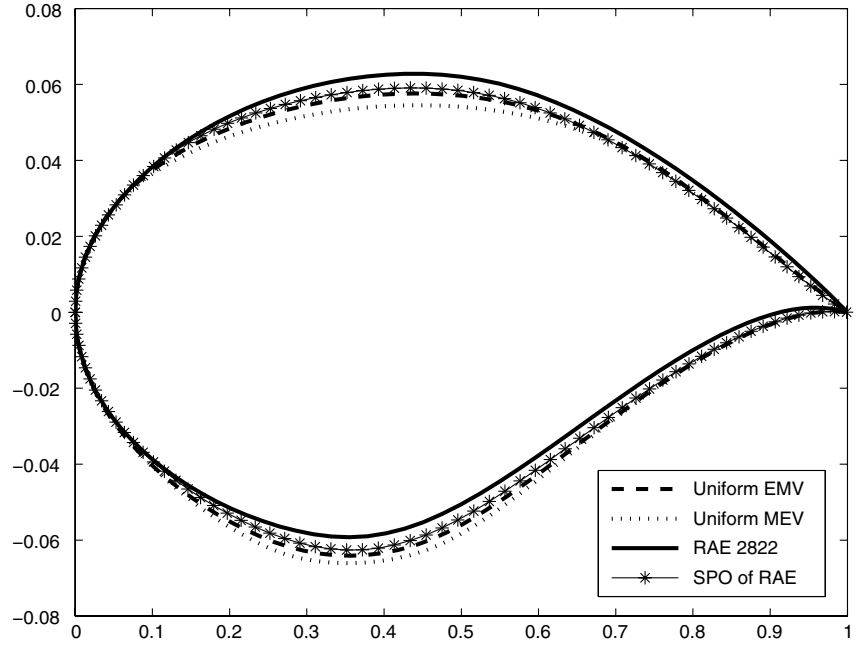

a) Airfoil shapes: RAE 2822 and three optimizations, 5× exaggerated thickness

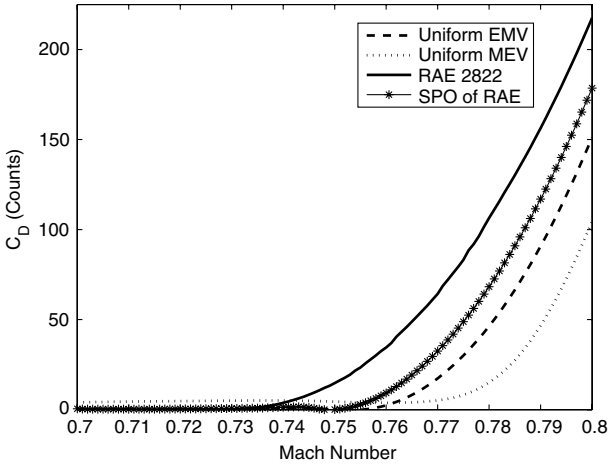

b) Drag coefficient

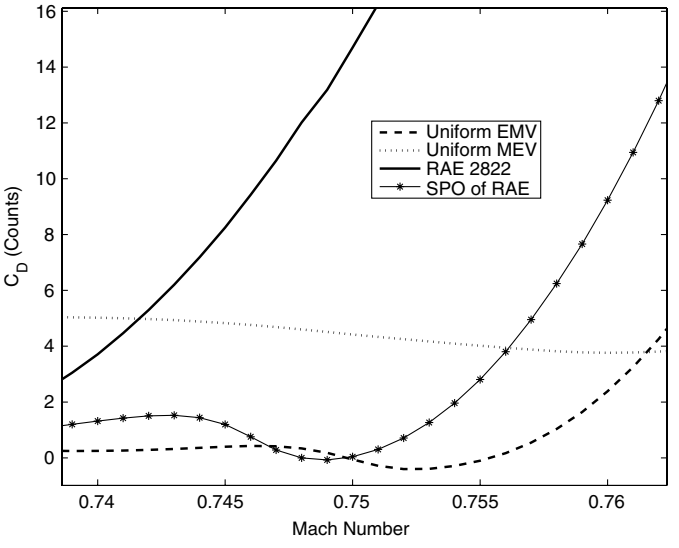

c) Drag coefficient, detail at mean M

Fig. 2 Shape and drag coefficient for uniform $M \sim \mathcal{U}[0.7, 0.8]$.

found in the literature, and they are concerned with an optimal design that is robust to small manufacturing errors or fluctuations in operating conditions, such as the cruise Mach number. In the context of this paper, robust design refers to a design for which the performance of the optimized shape is relatively insensitive to random variations in the uncertain parameters. This research deals with designing a robust airfoil shape that reduces the drag coefficient over a range of freestream Mach numbers. The range of Mach number is due to the aleatory nature of the freestream uncertainties. For example, the naturally occurring, random nonuniformity of the freestream pressure, density, or temperature will cause aleatory uncertainty in the Mach number.

A single-point optimization (SPO) method can be employed as a tool for optimization under uncertainty [17–19], but the drag reduction is attained only over a narrow range of Mach numbers. An improved drag coefficient can be realized over a wider range of Mach numbers if multipoint optimization techniques are applied. With the multipoint formulation, practical problems arise with the selection of flight conditions and the specification of weights, which is left up to the designer's discretion [17–19].

Another possible approach is based on Von-Neumann–Morgenstern statistical decision theory, which is about choosing an optimal design that minimizes the expected drag in incompletely known situations. By Von Neumann and Morgenstern statistical decision theory (1944), there exists a utility function representing the decision maker risk preferences for an uncertain prospect, and the agent make decisions to maximize the expected utility of the uncertain prospect. This approach is commonly known as the maximum/minimum expected value (MEV) criterion, and its application to airfoil design is presented by Huyse et al. [17–19]. Later approaches, called the profile optimization method and the modified profile optimization method, are developed for achieving consistent drag reduction over a given Mach range with far fewer design points than are required for the multipoint optimization

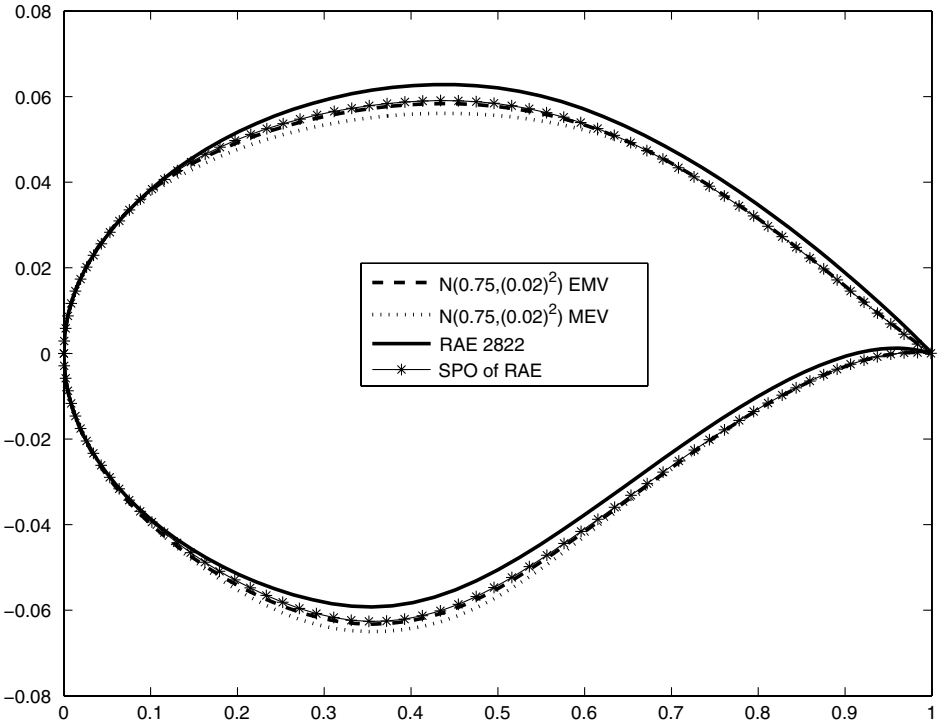

a) Airfoil shapes: RAE 2822 and three optimizations, 5× exaggerated thickness

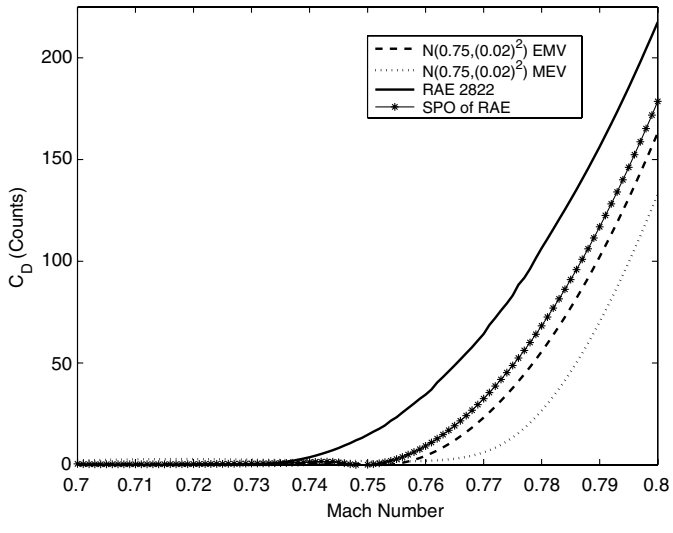

b) Drag coefficient

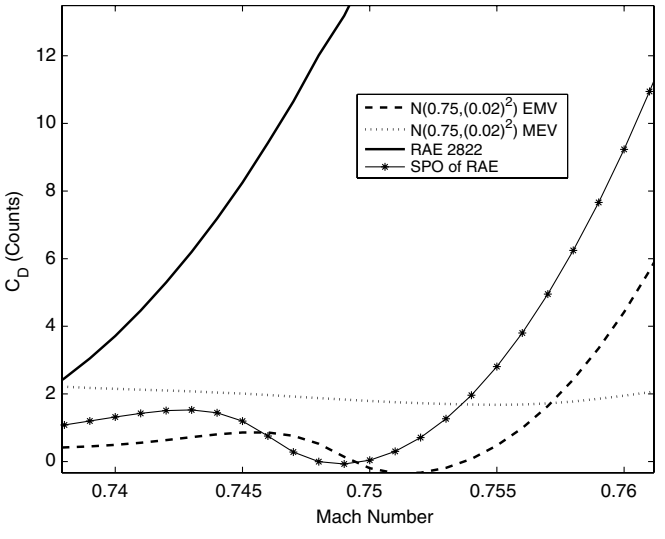

c) Drag coefficient, Detail at Mean M

Fig. 3 Shape and drag coefficient for Gaussian $M \sim \mathcal{N}[0.75, (0.02)^2]$.

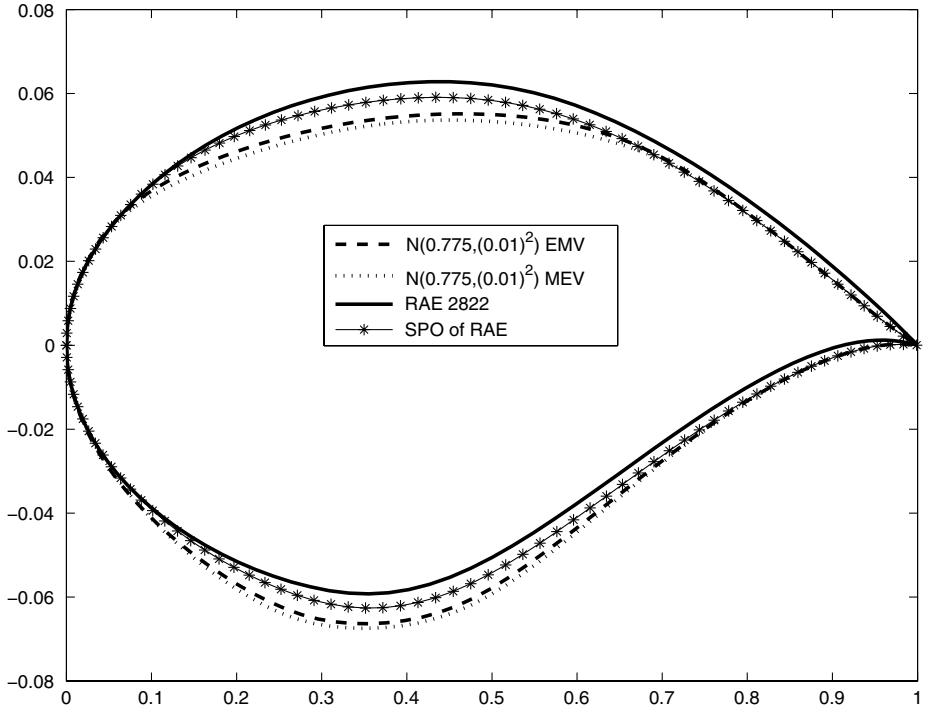

a) Airfoil shapes: RAE 2822 and three optimizations, 5× exaggerated thickness

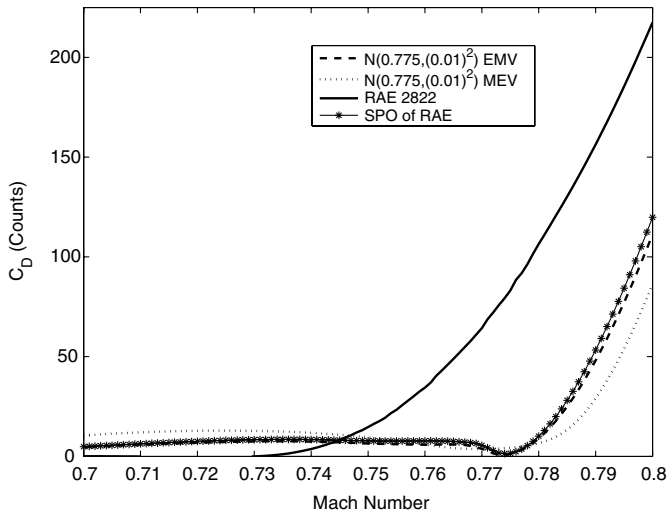

b) Drag coefficient

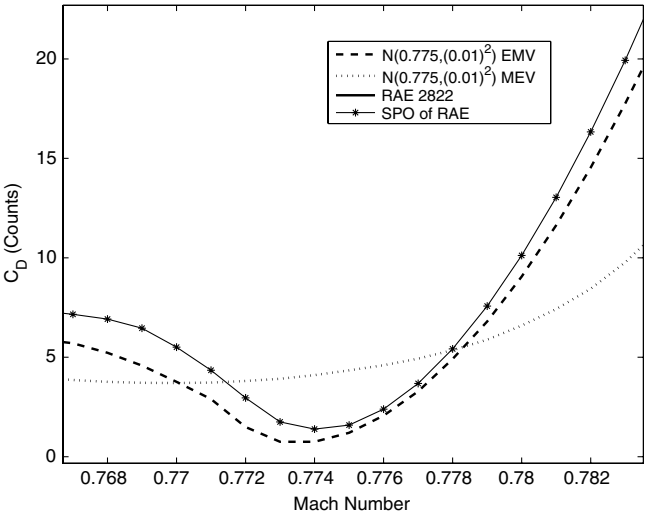

c) Drag coefficient, detail at mean M

Fig. 4 Shape and drag coefficient for Gaussian $M \sim \mathcal{N}[0.775, (0.01)^2]$.

technique [20–22]. One drawback of the profile optimization method is the greater likelihood of getting trapped in a local solution than the multipoint method.

The purpose of this paper is to demonstrate the potential of an easy way to implement an airfoil optimization scheme that achieves a consistent drag reduction over a given Mach number range. The expectation of the best designs, a so-called expected maximum/minimum value (EMV) criterion, inspired by the heuristic weighted average of geometries approach of Campbell [23], is discussed and analyzed as opposed to the widely accepted MEV criterion. The analysis is done for inviscid flow to demonstrate the viability of the EMV approach.

II. Problem Formulation: Airfoil Shape Optimization Under Uncertainty in the Operating Conditions

In this section we describe in more detail the aerodynamic problem under consideration. Generally speaking, our main objective is to find the optimal shape **d** of a two-dimensional airfoil over a range of cruise Mach numbers M. In other words, our goal is to minimize the drag coefficient C_D subject to a prescribed lift coefficient C_L^*, and some other geometrical constraints h_i, i.e.,

$$\min_{\mathbf{d}\in\mathbf{D}} C_D(\mathbf{d}, M), \text{over a range of } M \quad \text{subject to}$$
$$C_L = C_L^* \quad \text{and} \quad h_i(\mathbf{d}, M) \geq 0, \quad \text{for} \quad i = 1, 2, \ldots, n \quad (1)$$

The desired shape **d** is an element of a design space **D**, and the random Mach number M is defined on a given probability space $(\Omega, \mathcal{F}, P)$ with probability density function $f(M)$. We will use the compressible Euler equations as the mathematical model of the governing equations of the flow.

The optimization problem (1) carried out over a single value of the Mach number M is deterministic, as it does not take into account any probabilistic properties of the random variable M. The deterministic optimum shape can be determined using control theory approach, which has dramatic computational advantages over the finite

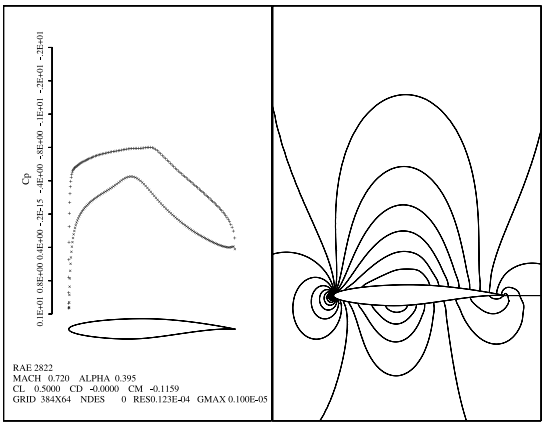

a) RAE 2822

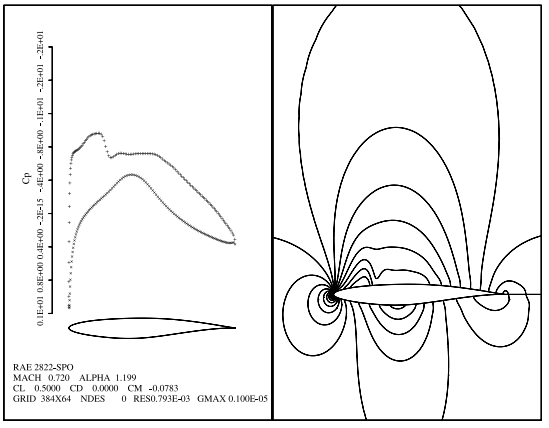

b) SPO

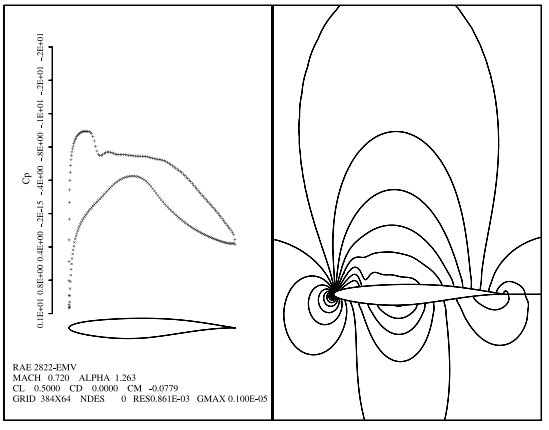

c) EMV

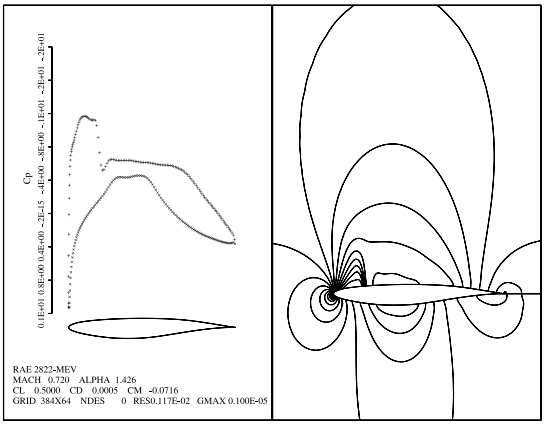

d) MEV

Fig. 5 Pressure distribution for RAE 2822 and three optimizations at $M = 0.72$ for uniform $M \sim \mathcal{U}[0.7, 0.8]$.

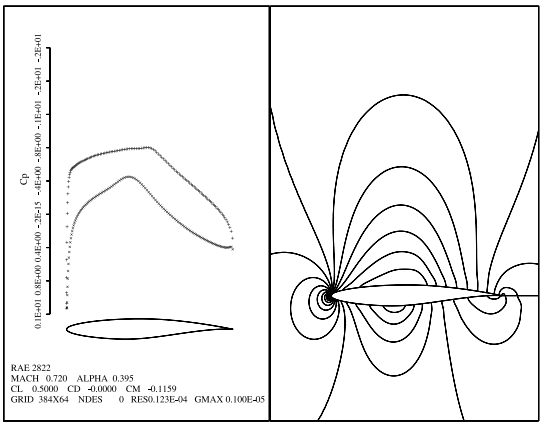

a) RAE 2822

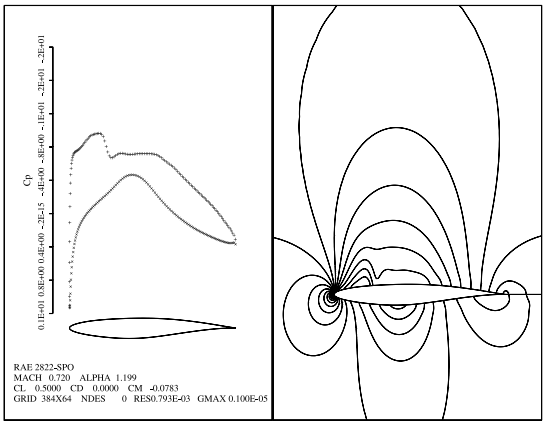

b) SPO

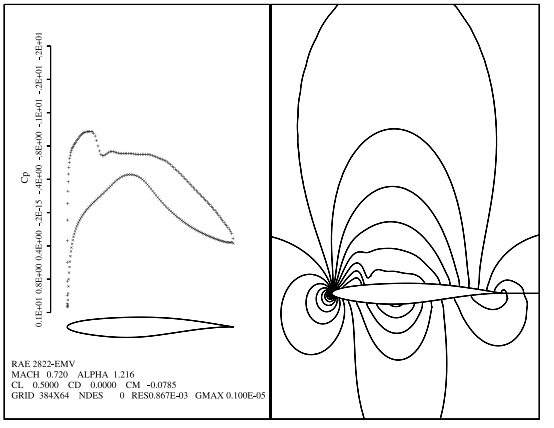

c) EMV

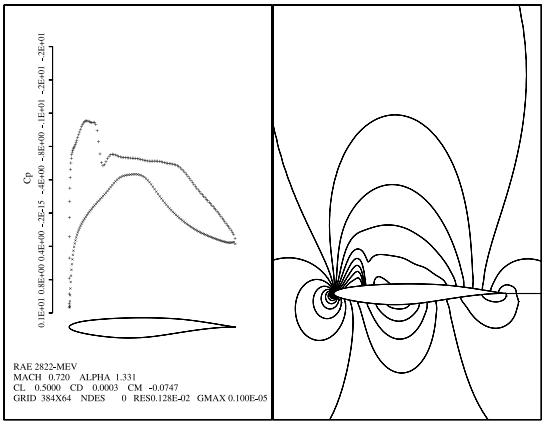

d) MEV

Fig. 6 Pressure distribution for RAE 2822 and three optimizations at $M = 0.72$ for Gaussian $M \sim \mathcal{N}[0.75, (0.02)^2]$.

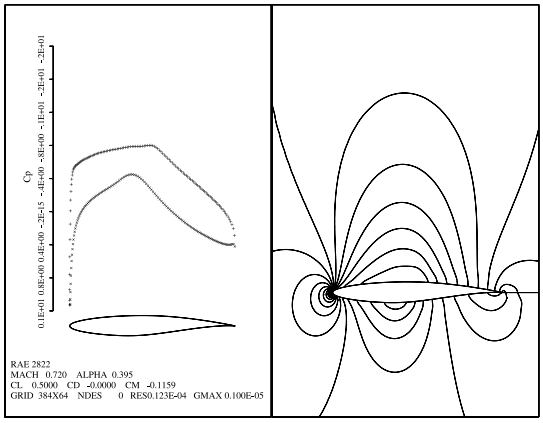

a) RAE 2822

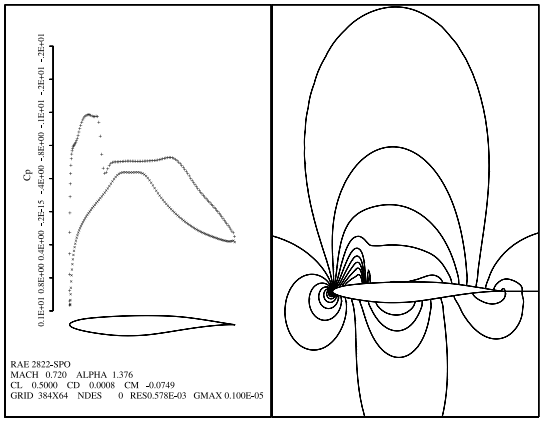

b) SPO

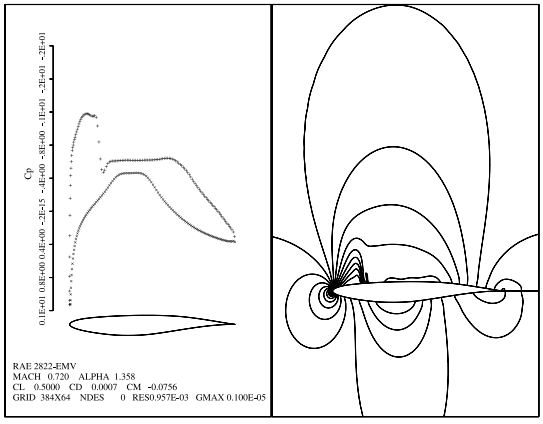

c) EMV

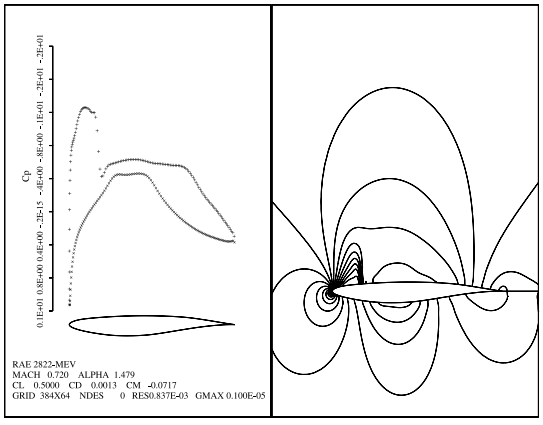

d) MEV

Fig. 7 Pressure distribution for RAE 2822 and three optimizations at $M = 0.72$ for Gaussian $M \sim \mathcal{N}[0.775, (0.01)^2]$.

differenced, gradient-based optimization methods. The governing equations of the flowfield are introduced as a constraint in such a way that the final expression for the gradient of the objective function does not require reevaluation of the flowfield. To achieve this purpose, a Lagrange multiplier (or costate variable) is introduced to satisfy the so-called adjoint equation [12]. Therefore, the design procedure can be described as follows:

1) Initialize the deterministic parameters involved in the optimization procedure, parameterize the configuration of interest using a set of design parameters, and define the initial shape.

2) Solve the flow equations for the flow variables density ρ, velocity components u_1, u_2, u_3, and pressure p.

3) Solve the adjoint equations for the costate variables subject to appropriate boundary conditions.

4) Evaluate the gradients and update the aerodynamic shape based on the direction of steepest descent (for instance).

5) Return to step 2 until an optimum configuration is attained.

Practical examples indicate that the deterministic optimization approach described previously can result in dramatically inferior performance when the actual operating conditions are different from the design values used for the optimization [1,2,18]. Therefore, practical robust designs need to be considered for achieving consistent drag reduction over a given Mach number range.

III. EMV and MEV Approach to Airfoil Shape Optimization Under Uncertainty

The problem of optimization under uncertainty (1) is quite challenging because it requires finding an optimum point that minimizes the objective function over a range of Mach numbers M. In general, one may find different designs associated with different values of M. To achieve well-posedness, the optimization problem (1) can be reformulated in the following ways/according to the following objectives [18,20]:

1) Find the design that minimizes the variance of the objective function (this is the goal of Taguchi methods [24]).

2) Find the worst-case performance (this is the objective of MiniMax strategies [25]).

3) Find the design that minimizes the expectation of the objective function (this is the objective of the Von-Neumann–Morgenstern statistical decision theory [26]).

4) Find the design that improves the performance over a given range of uncertain parameters compared to the MEV design (this is the objective of the present work).

We show that a so-called EMV criterion can be used for optimization under uncertainty (1). Croicu and Hussaini [27] have proven that in some illustrative cases, the EMV method provides a higher probability of lower objective function than the MEV approach. In terms of our optimization problem, that would be

$$P[C_D(\mathbf{d}_{\text{EMV}}, M) \leq C_D(\mathbf{d}_{\text{MEV}}, M)] \geq 50\%$$

It is interesting to analyze how the EMV compares to the MEV optimum solution in this aerodynamic shape design under uncertainty, especially because we are concerned with obtaining improvements to the airfoil geometry over a range of Mach numbers (see goal 4 mentioned previously).

Let us describe the two optimization strategies next.

A. EMV

The EMV optimum shape is defined to be

$$\mathbf{d}_{\text{EMV}} = E[\arg\min_{\mathbf{d}\in\mathbf{D}} C_D(\mathbf{d}, M)] = \int_{\Omega} \arg\min_{\mathbf{d}\in\mathbf{D}} C_D(\mathbf{d}, M) f(M)\, \mathrm{d}M \tag{2}$$

Because the function $M \mapsto \arg\min_{\mathbf{d}\in\mathbf{D}} C_D(\mathbf{d}, M)$ is continuous over Ω and the function $M \mapsto f(M)$ is continuous and positive on Ω, according to the second mean value theorem for integrals, there exists a value $M^* \in \Omega$ such that

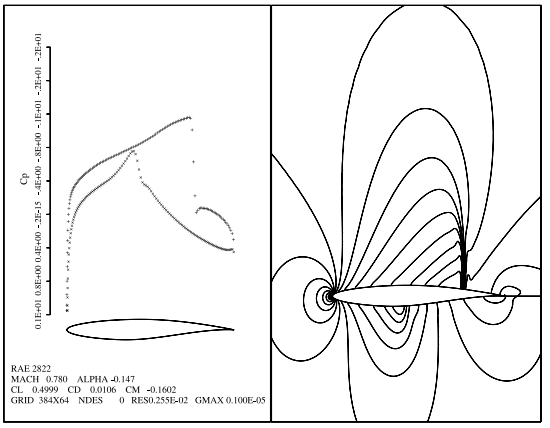

a) RAE 2822

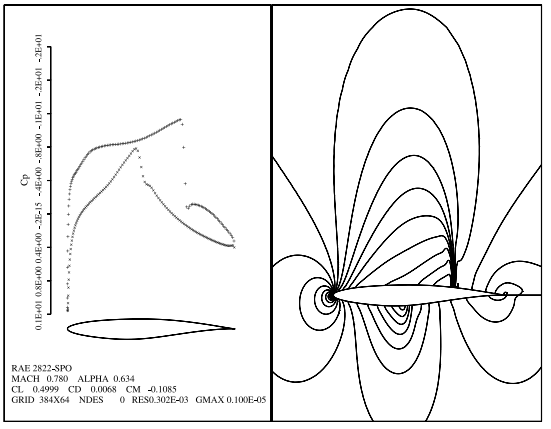

b) SPO

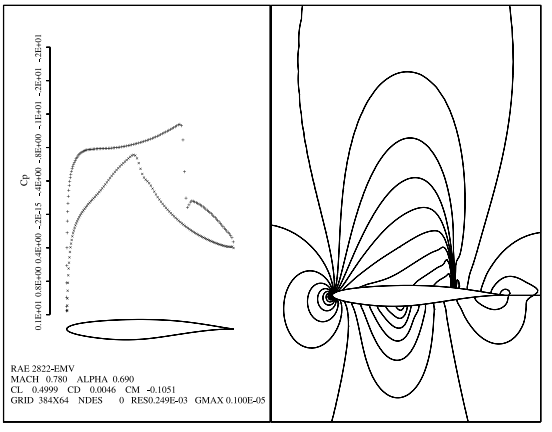

c) EMV

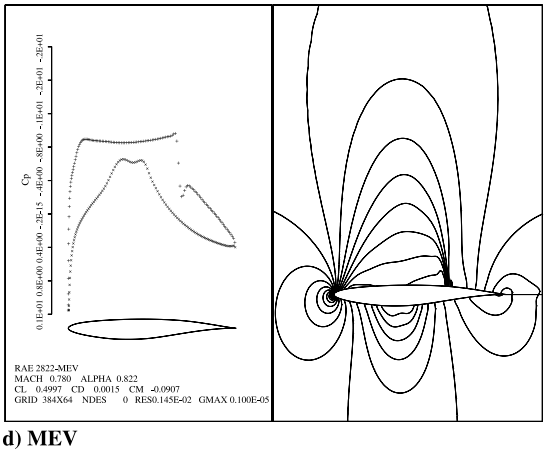

d) MEV

Fig. 8 Pressure distribution for RAE 2822 and three optimizations at $M = 0.78$ for uniform $M \sim \mathcal{U}[0.7, 0.8]$.

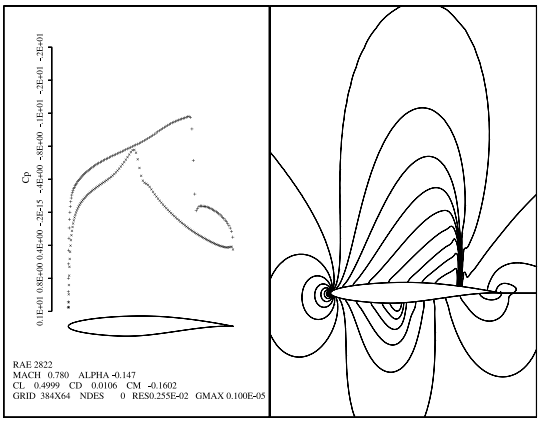

a) RAE 2822

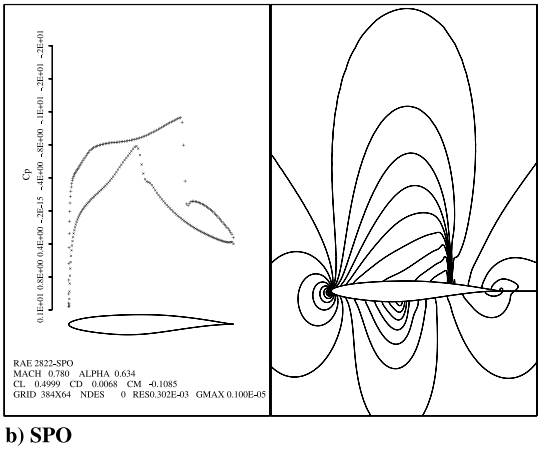

b) SPO

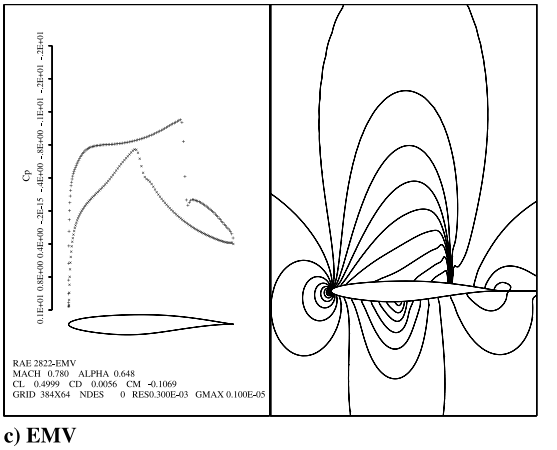

c) EMV

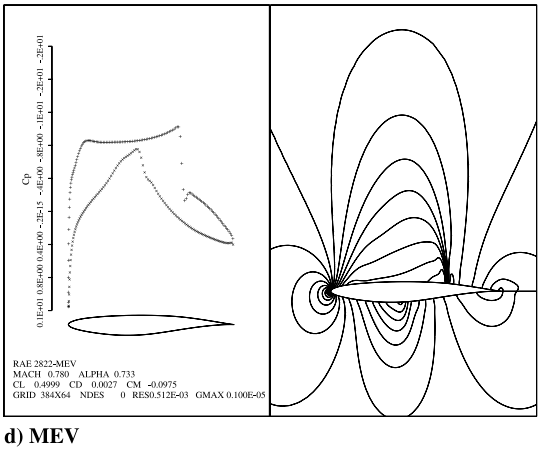

d) MEV

Fig. 9 Pressure distribution for RAE 2822 and three optimizations at $M = 0.78$ for Gaussian $M \sim \mathcal{N}[0.75, (0.02)^2]$.

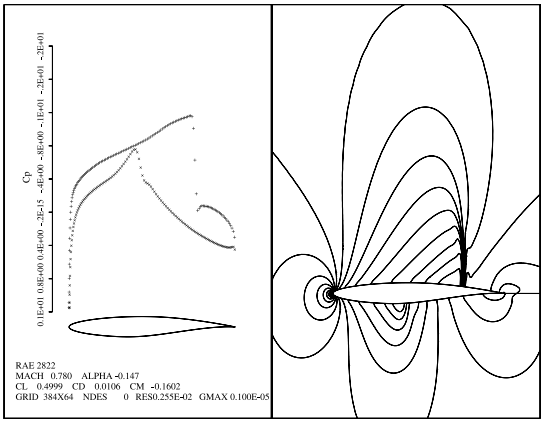

a) RAE 2822

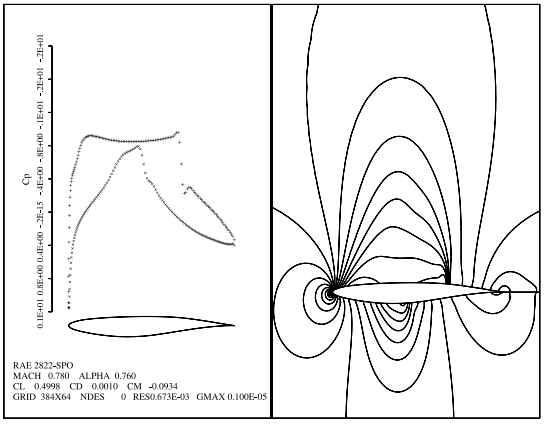

b) SPO

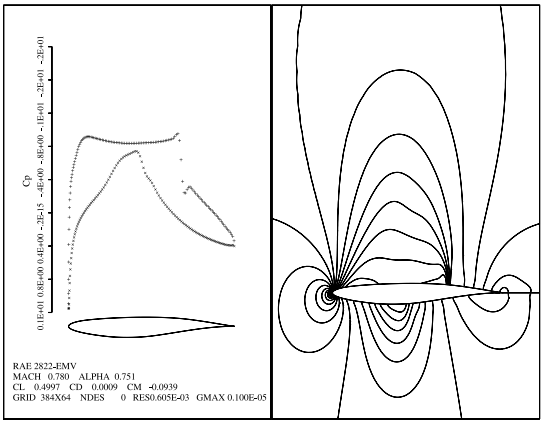

c) EMV

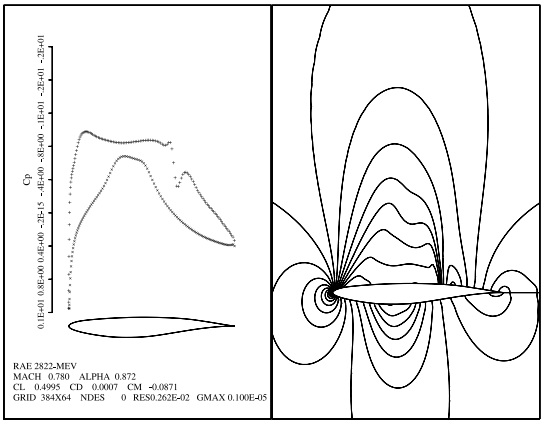

d) MEV

Fig. 10 Pressure distribution for RAE 2822 and three optimizations at $M = 0.78$ for Gaussian $M \sim \mathcal{N}[0.775, (0.01)^2]$.

$$\int_\Omega \arg\min_{\mathbf{d}\in\mathbf{D}} C_D(\mathbf{d}, M) f(M)\, \mathrm{d}M = \arg\min_{\mathbf{d}\in\mathbf{D}} C_D(\mathbf{d}, M^*) \int_\Omega f(M)\, \mathrm{d}M = \arg\min_{\mathbf{d}\in\mathbf{D}} C_D(\mathbf{d}, M^*)$$

It follows immediately from this argument that the EMV strategy exists and exhibits the good qualities of $\arg\min_{\mathbf{d}\in\mathbf{D}} C_D(\mathbf{d}, M^*)$, the optimal shape at M^*.

To approximate the right-hand side of Eq. (2), we let $M_1, M_2, \ldots, M_n$ be a random sample of size n of the random variable M with probability density function f. For each sample M_k, $k = 1, 2, \ldots, n$ value, the optimization problem (1) yields a solution $\mathbf{d}(M_k)$, $k = 1, 2, \ldots, n$. Therefore, the averaged optimal shape is considered to be

$$\mathbf{d}^{\,n}_{\mathrm{EMV}} = \frac{1}{n}\sum_{k=1}^{n} \mathbf{d}(M_k) = \frac{1}{n}\sum_{k=1}^{n} \arg\min_{\mathbf{d}\in\mathbf{D}} C_D(\mathbf{d}, M_k)$$

If the right-hand side of Eq. (2) is finite, then by the Strong Law of Large Numbers [28], the Monte Carlo type estimator $\mathbf{d}^{\,n}_{\mathrm{EMV}}$ converges to the desired optimum $\mathbf{d}_{\mathrm{EMV}}$, i.e.,

$$\mathbf{d}^{\,n}_{\mathrm{EMV}} \to \mathbf{d}_{\mathrm{EMV}} \quad \text{as} \quad n \to \infty$$

The overall design procedure can be summarized as follows:

1) Initialize the deterministic parameters, and parameterize the configuration of interest using a set of design variables.

2) Sample a value of the random parameter M, according to its probability distribution function (PDF) $f(M)$, and define the chosen initial shape.

3) Solve the flow equations for the flow variables ρ, u_1, u_2, u_3, p.

4) Solve the adjoint equations for the costate variables ψ subject to appropriate boundary conditions.

5) Evaluate the gradients G and update the aerodynamic shape based on the direction of steepest descent (for instance).

6) Return to step 3 until an optimum configuration is attained.

7) Return to step 2 and repeat until a desired number of sample points are analyzed.

8) Average all the optimum configurations obtained in step 6 to determine the EMV optimum design.

B. MEV

The MEV optimum shape, which is defined by Huyse et al. [17–19] to be

$$\mathbf{d}_{\mathrm{MEV}} = \arg\min_{\mathbf{d}\in\mathbf{D}} E[C_D(\mathbf{d}, M)] = \arg\min_{\mathbf{d}\in\mathbf{D}} \int_\Omega C_D(\mathbf{d}, M) f(M)\, \mathrm{d}M \tag{3}$$

is analyzed here too. In the same fashion as in the previous case, a Monte Carlo-type estimator defined by

$$\mathbf{d}^{\,n}_{\mathrm{MEV}} = \arg\min_{\mathbf{d}\in\mathbf{D}} \left[\frac{1}{n}\sum_{k=1}^{n} C_D(\mathbf{d}, M_k)\right]$$

converges to the optimum $\mathbf{d}_{MEV}$, as $n \to \infty$.

Because we would like to make use of a numerical deterministic code that minimizes the drag coefficient for known parameters, the procedure for implementing the MEV strategy could be described as follows:

1) Initialize the deterministic parameters, parameterize the configuration of interest using a set of design variables, and define the initial shape.

2) Sample all the values of the random variable M according to its PDF $f(M)$.

3) For every value of the random variable M, solve the flow equations for the flow variables ρ, u_1, u_2, u_3, p.

4) For every value of the random variable M and the current airfoil shape, solve the adjoint equations for the costate variables ψ subject to appropriate boundary conditions.

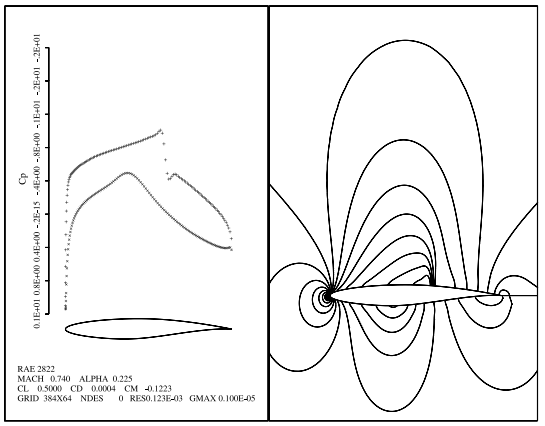

a) RAE2822

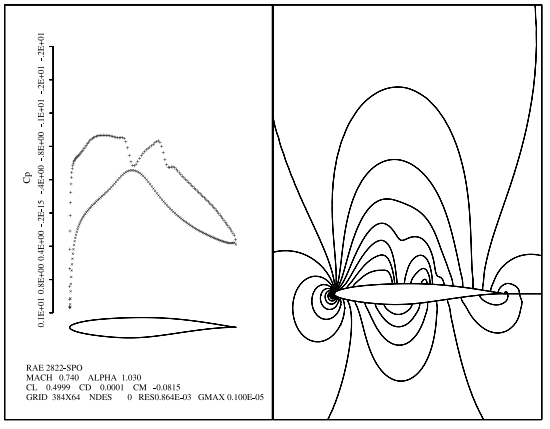

b) SPO

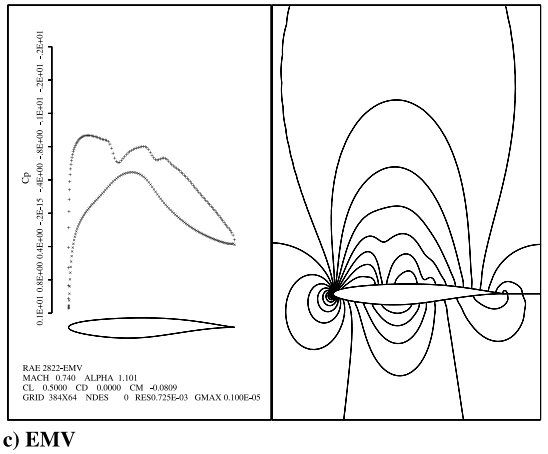

c) EMV

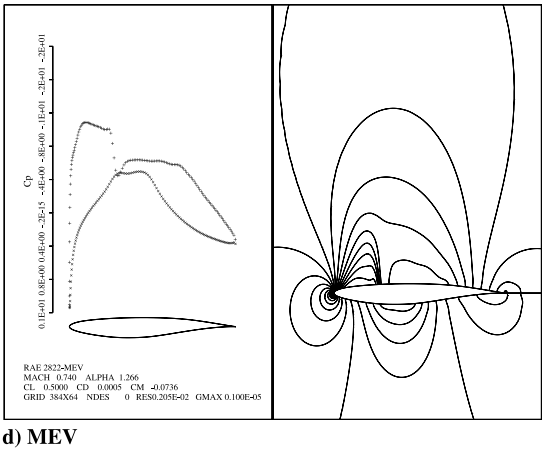

d) MEV

Fig. 11 Pressure distribution for RAE 2822 and three optimizations at $M = 0.74$ for uniform $M \sim \mathcal{U}[0.7, 0.8]$.

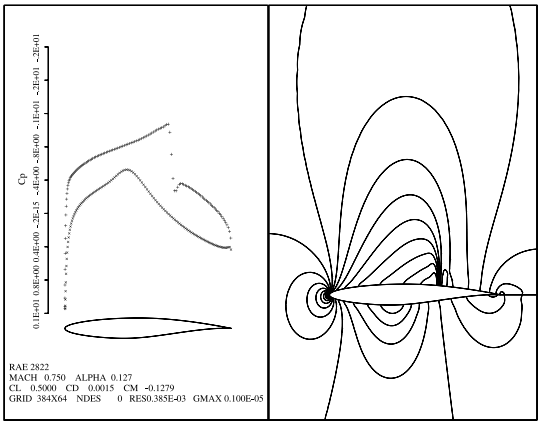

a) RAE 2822

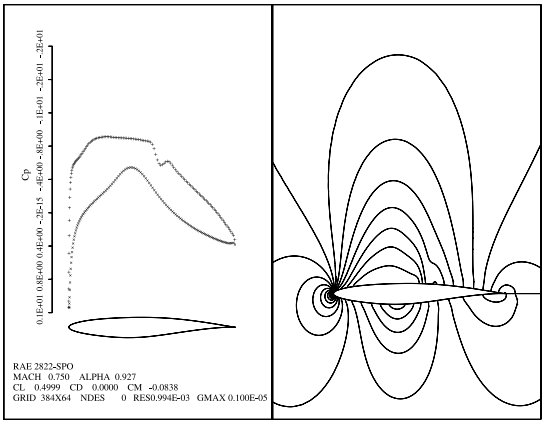

b) SPO

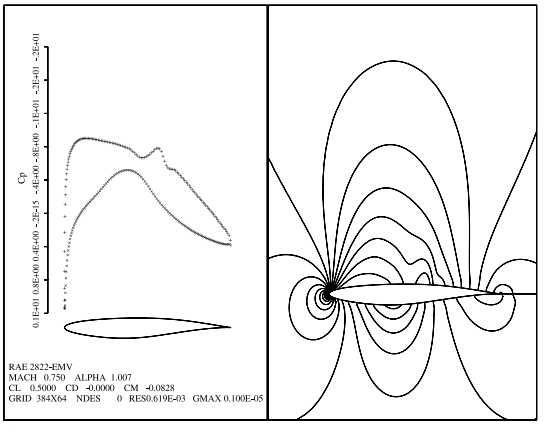

c) EMV

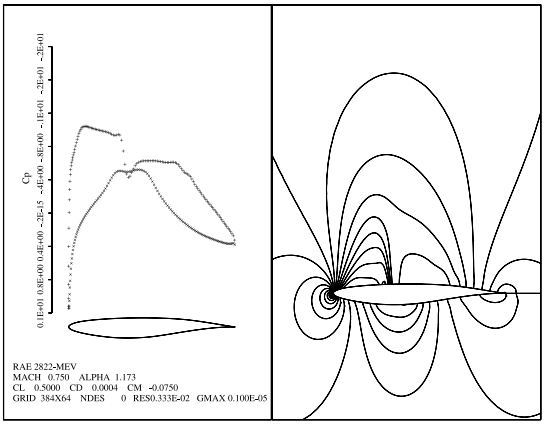

d) MEV

Fig. 12 Pressure distribution for RAE 2822 and three optimizations at $M = 0.75$ (mean) for uniform $M \sim \mathcal{U}[0.7, 0.8]$.

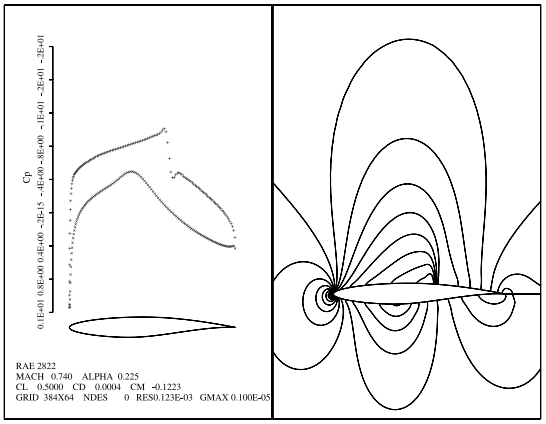

a) RAE 2822

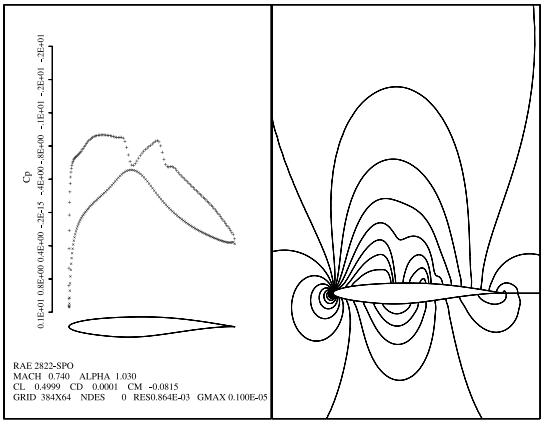

b) SPO

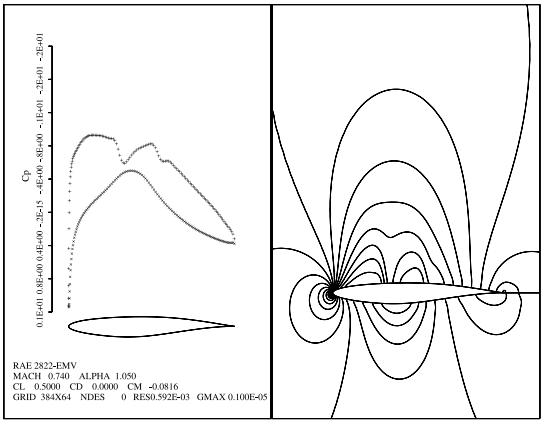

c) EMV

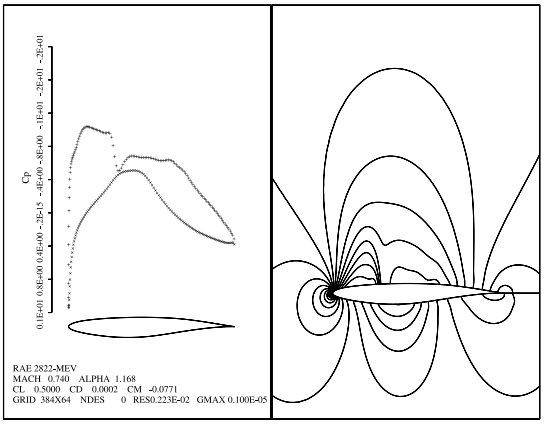

d) MEV

Fig. 13 Pressure distribution for RAE 2822 and three optimizations at $M = 0.74$ for Gaussian $M \sim \mathcal{N}[0.75, (0.02)^2]$.

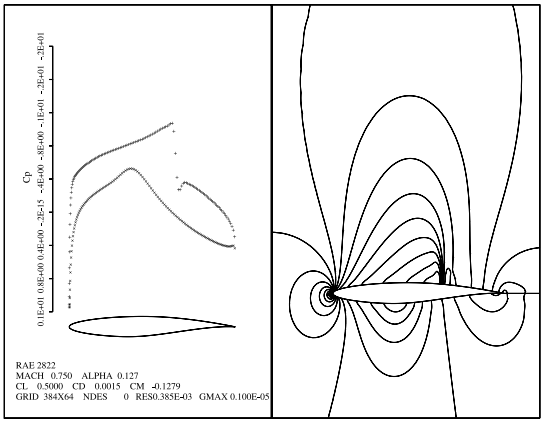

a) RAE 2822

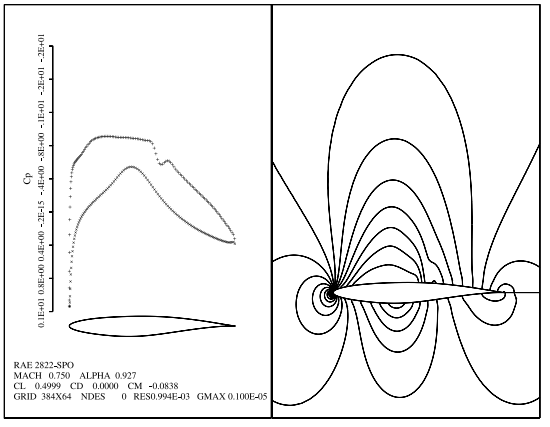

b) SPO

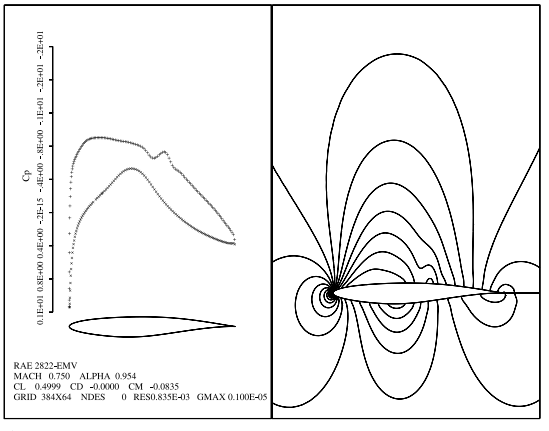

c) EMV

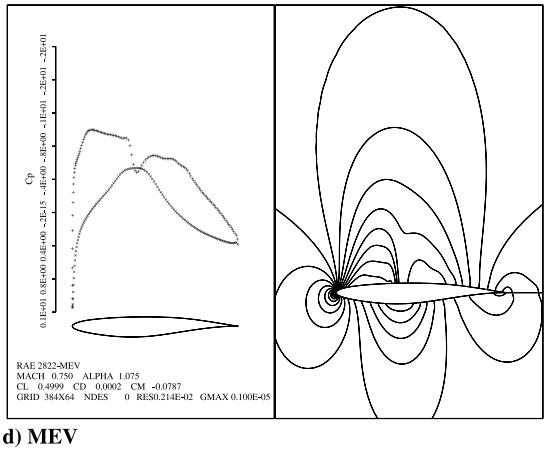

d) MEV

Fig. 14 Pressure distribution for RAE 2822 and three optimizations at $M = 0.75$ (mean) for Gaussian $M \sim \mathcal{N}[0.75, (0.02)^2]$.

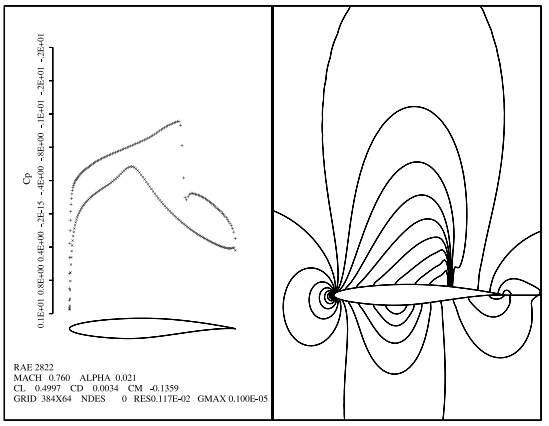

a) RAE 2822

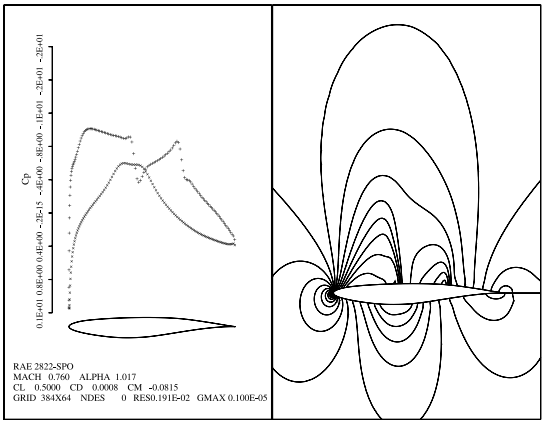

b) SPO

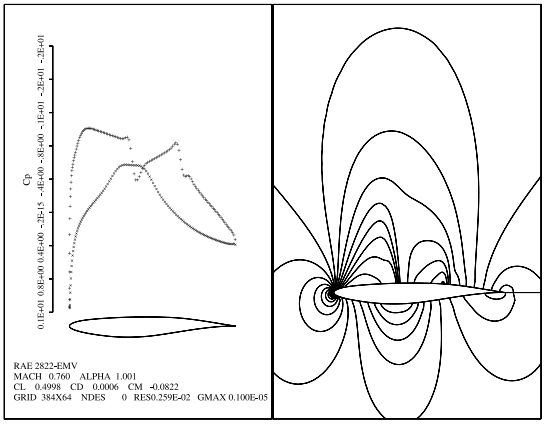

c) EMV

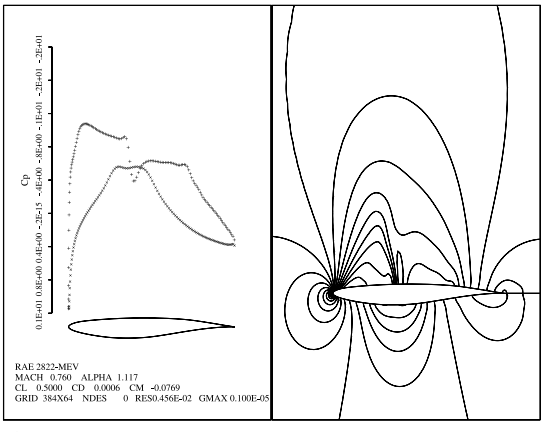

d) MEV

Fig. 15 Pressure distribution for RAE 2822 and three optimizations at $M = 0.76$ for Gaussian $M \sim \mathcal{N}[0.775, (0.01)^2]$.

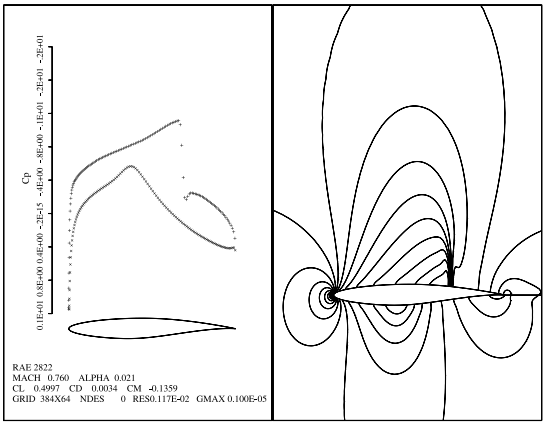

a) RAE 2822

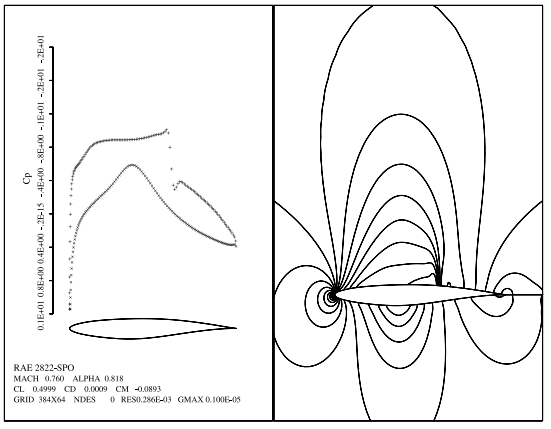

b) SPO

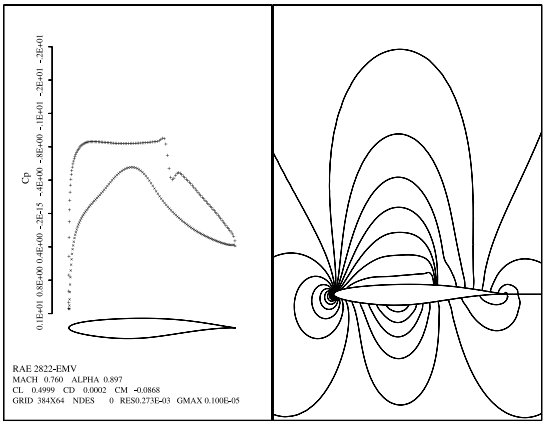

c) EMV

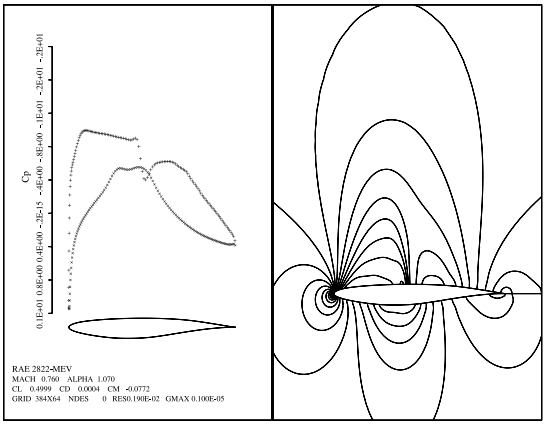

d) MEV

Fig. 16 Pressure distribution for RAE 2822 and three optimizations at $M = 0.76$ for uniform $M \sim \mathcal{U}[0.7, 0.8]$.

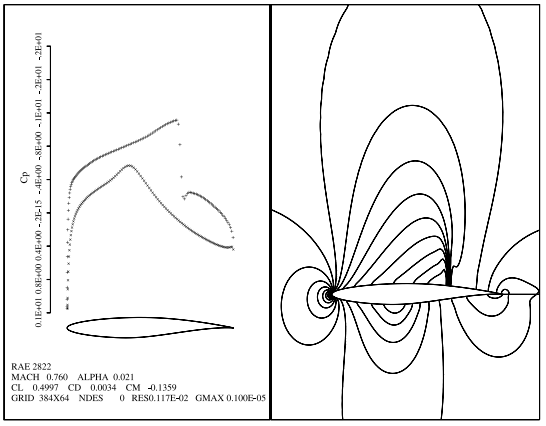

a) RAE 2822

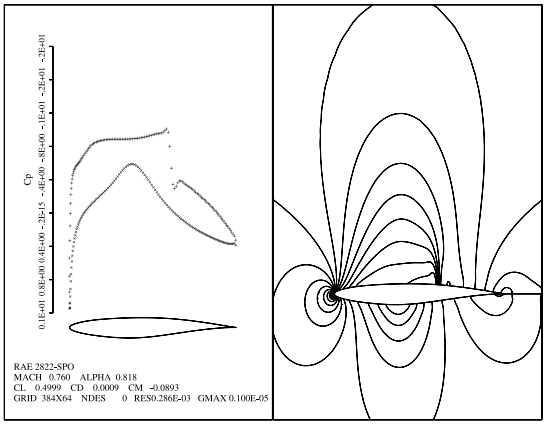

b) SPO

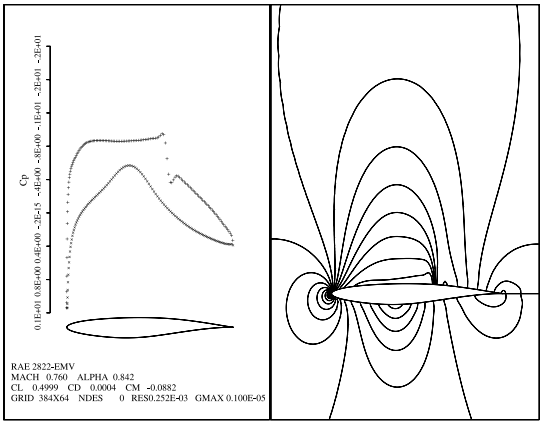

c) EMV

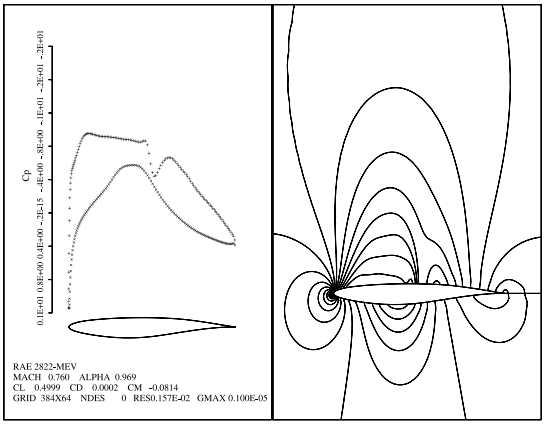

d) MEV

Fig. 17 Pressure distribution for RAE 2822 and three optimizations at $M = 0.76$ for Gaussian $M \sim \mathcal{N}[0.75, (0.02)^2]$.

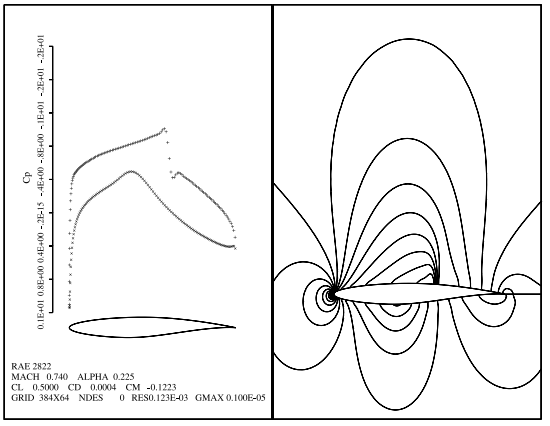

a) RAE 2822

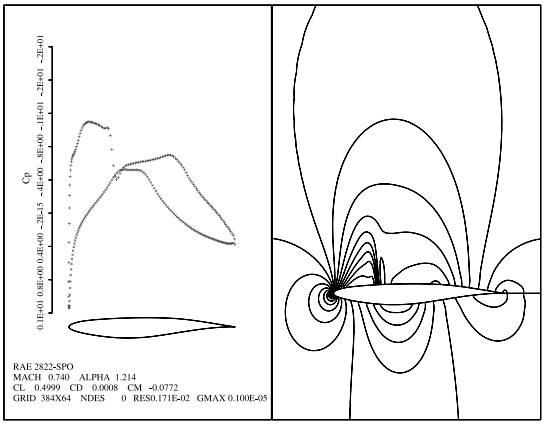

b) SPO

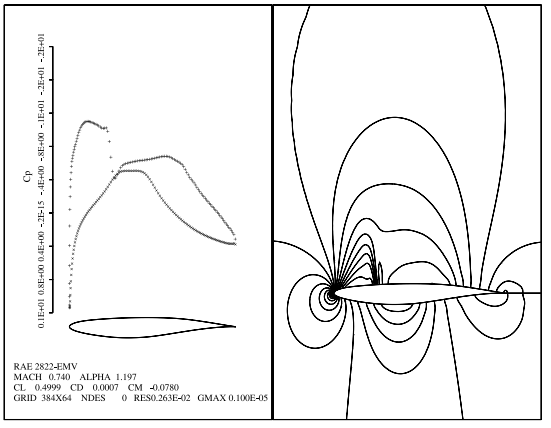

c) EMV

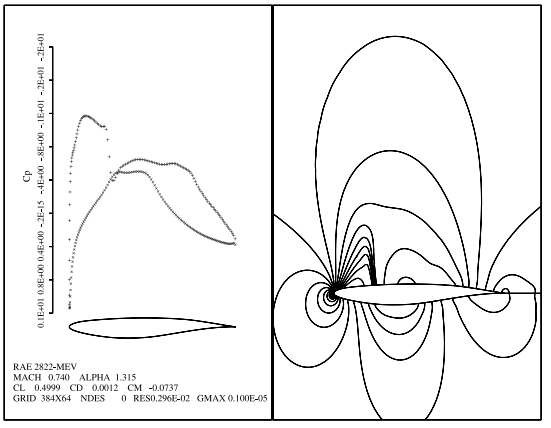

d) MEV

Fig. 18 Pressure distribution for RAE 2822 and three optimizations at $M = 0.74$ for Gaussian $M \sim \mathcal{N}[0.775, (0.01)^2]$.

5) Evaluate the gradients G for every value of the random variable M, average all the gradients and update the aerodynamic shape based on the averaged direction of steepest descent (for instance).

6) Return to step 3 and repeat until an MEV optimum configuration is attained.

As described herein and seen in the work of Huyse et al. [17,18], the MEV method is computationally similar to the multipoint optimization with the number of design points larger than the number of design parameters. According to Drela [2], sampling a larger number of operating points than design variables will provide a smooth MEV geometry (additional bumps that appear at the intermediate locations will blend into a smooth surface). Based on the same argument, we expect that an "average" of a large number of SPO bumpy airfoils will also blend into a smooth EMV profile.

IV. Results

The design of a transonic airfoil that performs well over a range of different Mach numbers is investigated using the EMV and MEV approaches and the computational fluid dynamics (CFD) code SYN83. Some technical details of SYN83 can be found in the work of Jameson [12].

SYN83 is an implementation of a gradient-based optimization technique in which the control variable (the airfoil shape $\mathbf{d}$) is parametrized using a set of 65 design nodes $\{(x_i, y_i), i = 1, 2, \ldots, 65\}$. The design nodes are the grid points along the surface of the airfoil. For a shape change, the design nodes are perturbed along the normal mesh lines, and then the whole grid is perturbed to conform to the shape change. Smooth shape changes are enforced by using a Sobolev gradient, which is equivalent to implicit smoothing of the gradient in a manner such that descent is still guaranteed. A thickness constraint is enforced by separating thickness and camber and then blocking any change that would reduce the thickness anywhere along the profile [29]. The drag coefficient is the objective function to be minimized. The gradient information is obtained via the adjoint equation, and this adjoint equation is used to calculate the sensitivity derivatives of the cost function with respect to the design variables, in order to get a direction of improvement. The flow is calculated using the steady-state inviscid Euler equations. The initial shape is the well-known RAE 2822 profile with an imposed lift coefficient $C_L = 0.5$ [30]. Because this shape is not suitable for the transonic regime, substantial improvements are to be expected. The number of iterations for the optimization algorithm, which is the stopping criterion implemented in the CFD code SYN83, is chosen to be 20. The design calculations are performed on a 192×32 mesh. Figure 1 shows that 20 design cycles are sufficient for a SPO on this relatively coarse grid. However, in order to verify the designs, subsequent analysis calculations are performed on a finer mesh of 384×64, which is able to capture the shock [30]. The same number of design cycles is used for the finer mesh, as convergence is achieved due to the use of Sobolev gradient [29].

We should mention that the specification of the Mach number is sufficient to carry out the optimal shape in the SYN83 code, and therefore the implementation of the EMV method is quite straightforward. The implementation of the MEV approach requires some modifications to the SYN83 source code.

We assume the following three distributions of the Mach number: uniform distribution $M \sim \mathcal{U}[0.7, 0.8]$, Gaussian distribution $M \sim \mathcal{N}[0.75, (0.02)^2]$, and Gaussian distribution $M \sim \mathcal{N}[0.775, (0.01)^2]$. Different distributions are chosen with the aim of emphasizing the importance of accurately quantifying the PDF of the Mach range. For practical problems, the PDF is likely to be very different from the distributions used in our numerical simulations. The actual PDF can be generated if appropriate historical flight data are available. The goal of finding realistic PDFs lies outside of the scope of the research presented here.

For both stochastic optimization procedures (EMV or MEV) and for each distribution, we choose 1000 samples of the Mach number. We note that a continuous objective function and a single stochastic

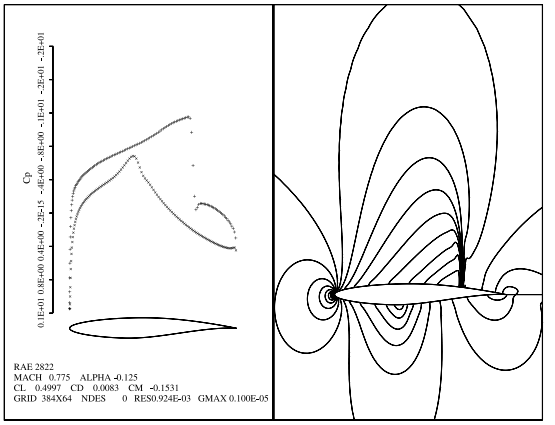

a) RAE 2822

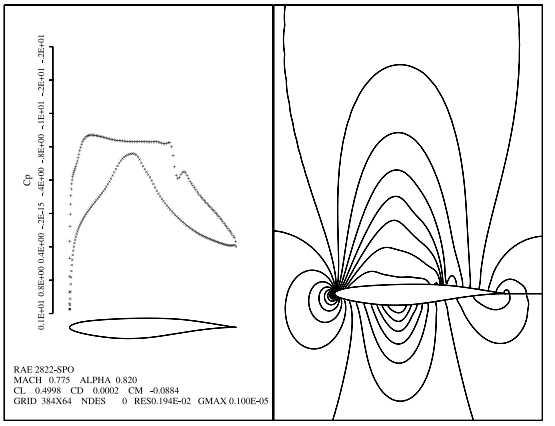

b) SPO

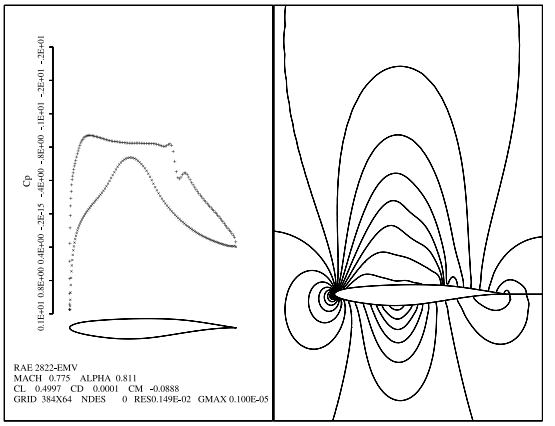

c) EMV

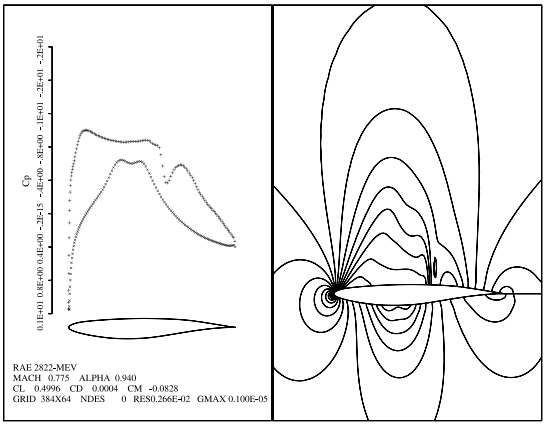

d) MEV

Fig. 19 Pressure distribution for RAE 2822 and three optimizations at $M = 0.775$ (mean) for Gaussian $M \sim \mathcal{N}[0.775, (0.01)^2]$.

Table 1 Expected drag coefficient (counts) for RAE 2822, EMV, MEV, and SPO over [0.7,0.8]

Distribution	RAE 2822	EMV	MEV	SPO
Uniform $M \sim \mathcal{U}[0.7, 0.8]$	48.9490	23.3369	14.6709	31.9309
Gaussian $M \sim \mathcal{N}[0.75, (0.02)^2]$	30.1773	11.1388	6.7899	14.6722
Gaussian $M \sim \mathcal{N}[0.775, (0.01)^2]$	88.3768	12.7677	9.4013	14.6763

parameter allow the use of a stochastic collocation method. However, this method was not used since the flowfield has discontinuities and the stochastic collocation would not be applicable for determining the statistical properties of the pressure distribution, for example. Discontinuous stochastic collocation methods are currently being developed to accelerate convergence of EMV and MEV estimators [31].

An optimal shape is found using the EMV and the MEV methods, as well as an SPO at the mean of the Mach number distributions. To better compare these minimization procedures, we plotted the optimized profiles and pressure distributions and calculated the corresponding drag coefficient at 100 equally spaced points in [0.7, 0.8].

Figures 2–4 show a comparison of the shapes (the vertical axis is scaled up by a factor of five) and drag coefficients among the original RAE 2822, SPO at the mean value and EMV, MEV profiles for the aforementioned distributions. All figures show smoothly shaped airfoils like the ones obtained by Li and Padula [22]. The differences between the EMV and SPO designs are very small for the uniform $M \sim \mathcal{U}[0.7, 0.8]$, and normal distribution $M \sim \mathcal{N}[0.75, (0.02)^2]$, while the differences between the EMV and MEV profiles are very small for the normal distribution $M \sim \mathcal{N}[0.775, (0.01)^2]$. As expected, there is a dip in C_D at the mean of the Mach numbers for the SPO at that design point. A drag reduction is seen for both EMV and MEV profiles compared to the initial RAE 2822 and the SPO airfoil for all 3 M number distributions. The EMV optimal shape provides the best drag reduction at low Mach numbers, while the MEV optimal shape provides the lowest drag for high Mach numbers. Moreover, the EMV method gives us a profile that experiences approximately the same low drag at the mean value of the Mach number as the SPO design, and for more than 50% of the Mach numbers under consideration.

On the other hand, because of the wide range of possible Mach numbers and Mach number distributions, the performance of optimized EMV, MEV, and SPO profiles are more or less satisfactory than the original RAE 2822 performance.

Figures 5–7 show that the low-speed behavior of the SPO, EMV, and MEV is worse than the original airfoil, but at high speeds the performance is better, as shown by Figs. 8–10. At Mach 0.78, there is a shock wave on the lower surface of RAE 2822, SPO, and EMV profiles, but not on the lower surface of MEV, which provides the lowest drag of all profiles.

According to Figs. 11–14, EMV is a zero drag profile at Mach 0.74 and the mean Mach 0.75 for the uniform distribution $M \sim \mathcal{U}[0.7, 0.8]$ and normal distribution $M \sim \mathcal{N}[0.75, (0.02)^2]$. At Mach 0.74 for the uniform distribution $M \sim \mathcal{U}[0.7, 0.8]$ and normal distribution $M \sim \mathcal{N}[0.75, (0.02)^2]$, and at Mach 0.76 for the normal distribution $M \sim \mathcal{N}[0.775, (0.01)^2]$, a double shock pattern forms for the EMV and SPO profiles that was not present on the original airfoil (see Figs. 11, 13, and 15).

Figures 15–17 show that all profiles experience a shock at Mach 0.76, with EMV having the lowest drag for the uniform distribution $M \sim \mathcal{U}[0.7, 0.8]$ and MEV having the lowest drag for the normal distributions $M \sim \mathcal{N}[0.75, (0.02)^2]$ and $M \sim \mathcal{N}[0.775, (0.01)^2]$.

To compare the EMV and MEV even further, both profiles experience a shock wave starting at low Mach numbers (see Figs. 5–7 for $M \sim \mathcal{U}[0.7, 0.8]$, $M \sim \mathcal{N}[0.75, (0.02)^2]$, and $M \sim \mathcal{N}[0.775, (0.01)^2]$, respectively). The EMV profile experiences a smaller shock wave at the leading edge for low Mach numbers compared to the MEV candidate. With the increase of the Mach numbers, the shock wave travels to the trailing edge. See for example Figs. 11, 12, and 16 for the uniform distribution. The same trend is observed for the two normal distributions as shown in Figs. 13–15 and 17–19. The EMV profile experiences a stronger shock wave at large Mach numbers compared to the MEV geometry (see Figs. 8–10 for the three distributions, respectively).

In addition, the values of the expected drag restricted to the interval [0.7, 0.8], corresponding to the RAE 2822, EMV, MEV and SPO airfoils, are displayed in Table 1. The MEV profile provides the minimum expected value, followed by the EMV profile. The differences between the expected values are significant, showing once again the importance of aerodynamic design under uncertainty.

Finally, we should remark that, due to their formulation, both EMV and MEV strategies can get trapped in a local optimum. One might use multiple starting points for these strategies to avoid that type of trap. The CPU time needed to carry out the EMV and MEV optimizations is approximately 15,000 s, regardless of the type of sampling of the Mach number. All computations in this paper were performed in double precision (64-bit arithmetic) on a Dell PC (P4, 2.26 GHZ, 512 MB).

V. Conclusions

In this paper, we focused on obtaining a robust optimal design starting from an RAE 2822 airfoil with Mach number as an uncertain parameter. Two different stochastic approaches (EMV and MEV) have been investigated and compared to the deterministic SPO. As expected, the SPO degrades rapidly away from the design point and does not provide robust results under the uncertainty of the Mach number. The first stochastic approach, the EMV strategy, is easier to implement if a deterministic optimization code is available. We showed that EMV provides lower drag for low speeds, lower drag for more than 50% of the Mach range, and similar performance to the SPO profile at the mean Mach design point. Additionally, we showed that the MEV profile exhibits lower drag at high speeds and the lowest expected drag. In conclusion, the appropriate choice between the EMV and MEV strategies depends on many considerations. The magnitude of the shock waves, the most plausible speed regime and speed distribution, the ease of computational implementations are only a few considerations that need to be taken into account when selecting between the EMV and MEV optimization methods.

Acknowledgments

This work was partially supported by the National Science Foundation under grant no. 0810875 and NASA Ames Research Center under Task 073: TN Visiting Scientists Program.

References

[1] Drela, M., "Low Reynolds Number Airfoil Design for the MIT Deadalus Prototype: A Case Study," *Journal of Aircraft*, Vol. 25, No. 8, 1988, pp. 724–732. doi:10.2514/3.45650

[2] Drela, M., "Pros and Cons of Airfoil Optimization," *Frontiers of Computational Fluid Dynamics*, edited by D. A. Caughey and M. M. Hafez, World Scientific, Hackensack, NJ, 1998, pp. 363–381.

[3] Kim, S., Alonso, J. J., and Jameson, A., "Two-Dimensional High-Lift Aerodynamic Optimization Using the Continuous Adjoint Method," AIAA Paper 2000-4741, Sept. 2000.

[4] Kim, S., Alonso, J. J., and Jameson, A.,"Design Optimization of High-Lift Configurations Using a Viscous Continuous Adjoint Method," AIAA Paper 2002-0844, Jan. 2002.

[5] Jameson, A., and Kim, S., "Reduction of the Adjoint Gradient Formula for Aerodynamic Shape Optimization Problems," *AIAA Journal*, Vol. 41, No. 11, 2003, pp. 2114–2129. doi:10.2514/2.6830

[6] Kim, H.-J., Koc, S., and Nakahashi, K., "Surface Modification Method for Aerodynamic Design Optimization," *AIAA Journal*, Vol. 43, No. 4, 2005, pp. 727–740. doi:10.2514/1.11181

[7] Wang, X., Damodaran, M., and Lee, S. L., "Inverse Transonic Airfoil Design Using Parallel Simulated Annealing and Computational Fluid Dynamics," *AIAA Journal*, Vol. 40, No. 4, 2002, pp. 791–794. doi:10.2514/2.1714

[8] de Sousa, F. L., and Ramos, M., "New Stochastic Algorithm for Design Optimization," *AIAA Journal*, Vol. 41, No. 9, 2003, pp. 1808–1818. doi:10.2514/2.7299

[9] Xing, X. Q., and Damodaran, M., "Application of Simultaneous Perturbation Stochastic Approximation Method for Aerodynamic Shape Design Optimization," *AIAA Journal*, Vol. 43, No. 2, 2005, pp. 284–294. doi:10.2514/1.9484

[10] Liu, J.-L., "Intelligent Genetic Algorithm and its Application to Aerodynamic Optimization of Airplanes," *AIAA Journal*, Vol. 43, No. 3, 2005, pp. 530–538. doi:10.2514/1.7070

[11] Pironneau, O., *Optimal Shape Design for Elliptic Systems*, Springer–Verlag, New York, 1984.

[12] Jameson, A., "Aerodynamic Design via Control Theory," *Journal of Scientific Computing*, Vol. 3, No. 3, 1988, pp. 233–260. doi:10.1007/BF01061285

[13] Quagliarella, D., and Cioppa, A. D., "Genetic Algorithms Applied to the Aerodynamic Design of Transonic Airfoils," AIAA Paper 1994-1896, June 1994.

[14] Yamamoto, K., and Inoue, O., "Applications of Genetic Algorithm to Aerodynamic Shape Optimization," *12th AIAA Computational Fluid Dynamics Conference*, CP956, AIAA, Washington, D.C., 1995, pp. 43–51.

[15] Aly, S., Ogot, M. M., and Pelz, R., "Stochastic Approach to Optimal Aerodynamic Shape Design," *Journal of Aircraft*, Vol. 33, No. 5, 1996, pp. 956–961. doi:10.2514/3.47041

[16] Kennedy, M. C., and O'Hagen, A.,"Bayesian Calibration of Computer Models," *Journal of the Royal Statistical Society. Series B*, Vol. 63, No. 3, 2001, pp. 425–464. doi:10.1111/1467-9868.00294

[17] Huyse, L., and Lewis, R. M., "Aerodynamic Shape Optimization of Two-Dimensional Airfoils Under Uncertain Conditions," ICASE Rept. No. 2001-1, NASA CR-2001-210648, Jan. 2001.

[18] Huyse, L., "Free-Form Airfoil Shape Optimization Under Uncertainty Using Maximum Expected Value and Second-Order Second-Moment Strategies," ICASE Rept. No. 2001-18, NASA CR-2001-211020, June 2001.

[19] Huyse, L., Padula, S. L., Lewis, R. M., and Li, W., "Uncertainty," *AIAA Journal*, Vol. 40, No. 9, 2002, pp. 1764–1772. doi:10.2514/2.1881

[20] Li, W., Huyse, L., and Padula, S., "Robust Airfoil Optimization to Achieve Drag Reduction Over a Range of Mach Numbers," *Structural and Multidisciplinary Optimization*, Vol. 24, No. 1, 2002, pp. 38–50. doi:10.1007/s00158-002-0212-4

[21] Li, W., "Profile Optimization Method for Robust Airfoil Shape Optimization in Viscous Flow," NASA TM-2003-212408, May 2003.

[22] Li, W., and Padula, S.,"Performance Trades Study for Robust Airfoil Shape Optimization," AIAA Paper 2003-3790, June 2003.

[23] Campbell, R. L., "Efficient Viscous Design of Realistic Aircraft Configurations," AIAA Paper 1998-2539, 1998.

[24] Fowlkes, W. Y., and Creveling, C. M., *Engineering Methods for Robust Product Design Using Taguchi Methods in Technological and Product Development*, Addison Wesley, Reading, MA, 1995.

[25] Ben-Tal, A., Nemirovski, A., "Robust Truss Topology Design via Semidefinite Programming," *SIAM Journal on Optimization*, Vol. 7, No. 4, 1997, pp. 991–1016. doi:10.1137/S1052623495291951

[26] Pratt, J. W., Raiffa, H., and Schlaifer, R., *Introduction to Statistical Decision Theory*, MIT Press, Cambridge, MA, 1995.

[27] Croicu, A.-M., and Hussaini, M. Y., "On the Expected Optimal Value and the Optimal Expected Value," *Applied Mathematics and Computation*, Vol. 180, No. 1, 2006, pp. 330–341. doi:10.1016/j.amc.2005.12.017

[28] Billingsley, P., *Probability and Measure*, Wiley, New York, 1986.

[29] Jameson, A., "Efficient Aerodynamic Shape Optimization," AIAA Paper 2004-4369, 2004.

[30] Harbeck, M., and Jameson, A., "Exploring the Limits of Shock-Free Transonic Airfoil Design," AIAA Paper 2005-1041, 2005.

[31] Barth, T. J., *UQ Methods for Nonlinear Conservation Laws Containing Discontinuities*, NATO RTO-VKI Lecture Series: Advanced Vehicle Technology AVT 193, Brussels, Belgium, Nov. 2011, http://www.rto.nato.int/ACTIVITY_META.asp?ACT=AVT-193 [retrieved 21 June 2012].

J. Martins
Associate Editor